

Determining the band alignment of TbAs:GaAs and TbAs:In_{0.53}Ga_{0.47}As

Cory C. Bomberger, Laura R. Vanderhoef, Abdur Rahman, Deesha Shah, D. Bruce Chase, Antoinette J. Taylor, Abul K. Azad, Matthew F. Doty, and Joshua M. O. Zide

Citation: [Applied Physics Letters](#) **107**, 102103 (2015); doi: 10.1063/1.4930816

View online: <http://dx.doi.org/10.1063/1.4930816>

View Table of Contents: <http://scitation.aip.org/content/aip/journal/apl/107/10?ver=pdfcov>

Published by the [AIP Publishing](#)

Articles you may be interested in

[Thermoelectric properties of epitaxial TbAs:InGaAs nanocomposites](#)

J. Appl. Phys. **111**, 094312 (2012); 10.1063/1.4711095

[Photoelectron spectroscopy study of band alignment at interface between Ni-InGaAs and In_{0.53}Ga_{0.47}As](#)

Appl. Phys. Lett. **99**, 012105 (2011); 10.1063/1.3607959

[Growth and characterization of TbAs:GaAs nanocomposites](#)

J. Vac. Sci. Technol. B **29**, 03C114 (2011); 10.1116/1.3555388

[Green's function approach for transport calculation in a In_{0.53}Ga_{0.47}As/In_{0.52}Al_{0.48}As modulation-doped heterostructure](#)

J. Appl. Phys. **93**, 3359 (2003); 10.1063/1.1555279

[Optical constants of In_{0.53}Ga_{0.47}As/InP : Experiment and modeling](#)

J. Appl. Phys. **92**, 5878 (2002); 10.1063/1.1515374

The advertisement for MMR Technologies features a blue and white background with a grid pattern. On the left is the MMR Technologies logo, which consists of a stylized 'M' and 'R' in a blue and red arc, with 'TECHNOLOGIES' written below. To the right of the logo is the text 'THE WORLD'S RESOURCE FOR VARIABLE TEMPERATURE SOLID STATE CHARACTERIZATION' in bold, black, uppercase letters. Below this text are five images of scientific equipment: 1. Optical Studies Systems, showing a small device and a larger unit. 2. Seebeck Studies Systems, showing a blue unit labeled 'SB1000' and 'K2000'. 3. Microprobe Stations, showing a circular device with multiple ports. 4. Hall Effect Study Systems and Magnets, showing a blue unit labeled 'H5000' and 'K2000' and a large magnet assembly. At the bottom left is the website 'WWW.MMR-TECH.COM' and at the bottom right is the text 'HALL EFFECT STUDY SYSTEMS AND MAGNETS'.

Determining the band alignment of TbAs:GaAs and TbAs:In_{0.53}Ga_{0.47}As

Cory C. Bomberger,¹ Laura R. Vanderhoef,² Abdur Rahman,³ Deesha Shah,⁴
 D. Bruce Chase,¹ Antoinette J. Taylor,⁴ Abul K. Azad,⁴ Matthew F. Doty,^{1,2}
 and Joshua M. O. Zide^{1,a)}

¹Department of Materials Science and Engineering, University of Delaware, Newark, Delaware 19716, USA

²Department of Physics and Astronomy, University of Delaware, Newark, Delaware 19716, USA

³Physics and Technology Department, Edinboro University of Pennsylvania, Edinboro, Pennsylvania 16444, USA

⁴Los Alamos National Laboratory, Los Alamos, New Mexico 87545, USA

(Received 28 July 2015; accepted 27 August 2015; published online 10 September 2015)

We propose and systematically justify a band structure for TbAs nanoparticles in GaAs and In_{0.53}Ga_{0.47}As host matrices. Fluence-dependent optical-pump terahertz-probe measurements suggest the TbAs nanoparticles have a band gap and provide information on the carrier dynamics, which are determined by the band alignment. Spectrophotometry measurements provide the energy of optical transitions in the nanocomposite systems and reveal a large blue shift in the absorption energy when the host matrix is changed from In_{0.53}Ga_{0.47}As to GaAs. Finally, Hall data provides the approximate Fermi level in each system. From this data, we deduce that the TbAs:GaAs system forms a type I (straddling) heterojunction and the TbAs:In_{0.53}Ga_{0.47}As system forms a type II (staggered) heterojunction. © 2015 AIP Publishing LLC. [<http://dx.doi.org/10.1063/1.4930816>]

Rare-earth monpnictides (RE-V) nanoparticles epitaxially embedded within III-V semiconductors are of great interest for a variety of devices. Specifically, TbAs and ErAs nanoparticles within In_{0.53}Ga_{0.47}As lattice matched to InP (here after referred to as InGaAs) improve the efficiency of thermoelectrics by increasing phonon scattering while maintaining high charge carrier mobility and electrical conductivity.^{1,2} ErAs nanoparticles improve the tunnel junctions in multijunction solar cells due to the formation of mid-gap states.^{3,4} ErAs nanoparticles in GaAs outperform state-of-the-art photoconductive switches for terahertz (THz) detection,⁵ and LaAs and GdAs nanoparticles in InGaAs are promising for terahertz generation.⁶ Recent work shows that core-shell TbErAs nanoparticles self assemble within an InGaAs matrix, providing the ability to tune electronic properties of nanoparticles and their interfaces for specific devices.⁷

To take advantage of the unique properties provided by RE-V nanoparticles and the ability to tune their properties for specific devices, a fundamental understanding of the electronic structure is needed. ErAs nanoparticles, which were believed to be very similar to TbAs, pin the Fermi level within the band gap of GaAs and above the conduction band edge in InGaAs.^{1,8–11} Cross-sectional scanning tunneling spectroscopy shows that ErAs nanoparticles are semi-metallic,¹² despite predictions that quantum confinement would open a band gap.¹³ Models of ErAs:GaAs superlattices show that interface states from the As atoms prevent the ErAs from transitioning from a semimetal into a semiconductor, even when the ErAs layer is reduced to one monolayer.¹⁴ Our recent carrier dynamics study shows that TbAs nanoparticles in GaAs are saturable, in direct contrast to ErAs nanoparticles, and likely have a band gap.¹⁵

Although TbAs nanoparticles are of interest for a variety of device applications, many details of their electronic structure in III-V semiconductors are presently unknown. In this paper we propose and systematically justify a type I heterojunction for the TbAs:GaAs system and a type II heterojunction for the TbAs:InGaAs system. We justify the proposed heterojunctions by demonstrating that they are consistent with the data from fluence-dependent optical-pump THz-probe measurements, spectrophotometry measurements, and Hall effect measurements.

For this work two samples were studied, a TbAs:GaAs sample and a TbAs:InGaAs sample. Both were grown in an OSEMI NextGEN solid source MBE. Details on the growths can be found elsewhere.^{2,15} The resulting TbAs:GaAs and TbAs:InGaAs films are 930 nm and 1.1 μm thick, respectively. Rutherford backscattering measurements reveals TbAs concentrations of 2.12% and 1.3%, respectively. Based on the growth conditions and average nanoparticle sizes measured from samples of similar growths,^{2,16} the calculated nanoparticle densities are $3.2 \times 10^{19} \text{ cm}^{-3}$ and $2.54 \times 10^{19} \text{ cm}^{-3}$ for TbAs:GaAs and TbAs:InGaAs, respectively.

Optical-pump THz-probe transient absorption spectroscopy was used to determine the carrier dynamics, including saturability, of TbAs nanoparticles epitaxially embedded in InGaAs; measurement details can be found elsewhere.¹⁵ Briefly, carriers are generated by an optical pulse and subsequently relax into the TbAs nanoparticle or back across the bulk band gap. The rate of the carrier relaxation is measured by the rate of decay in the absorption of a THz probe. The THz probe is only absorbed when free carriers are in the conduction or valence band. This absorption cannot distinguish electrons or holes and is a convolution of the two signals.

The time-dependent decay in THz absorption was measured for a range of optical pump fluences. Data for each set of experimental conditions were taken over multiple experimental runs, averaged, and fit to an exponential decay

^{a)}Electronic mail: zide@udel.edu

function. The triple exponential decay equation in Fig. 1(a) was used to fit the low fluence data where A_0 , A_1 , and A_2 are amplitude coefficients, providing information on the percentage of carriers participating in each relaxation process, and τ_0 , τ_1 , and τ_2 are the relaxation times for each process. Consistent with previous work on TbAs:GaAs,¹⁵ τ_0 has been assigned as relaxation into the TbAs nanoparticle, τ_1 as emptying the nanoparticle, and τ_2 as recombination across the InGaAs band gap. At higher fluences, the saturation of traps and neighboring states reduces the fraction of carriers participating in the fastest processes (τ_0 and τ_1) to a negligible level and double or single exponential fits are used. Example of triple, double, and single exponential decays (for different pump fluences) can be seen in the inset of Fig. 1(b).

The average relaxation time of carriers entering the TbAs nanoparticles is 4.6 ps and is independent of pump fluence, Fig. 1(a) solid black squares. However, the fraction of carriers entering the TbAs nanoparticles has a dependence on pump fluence, and reaches zero by $20 \mu\text{J}/\text{cm}^2$ pump

fluence, Fig. 1(b) solid black squares. This indicates that the nanoparticles' carrier capture rate does not change with pump fluence and the number of carriers that can relax into the nanoparticle is finite.

As carriers leave or recombine within the nanoparticle, additional carriers at the band edge can rapidly relax into the nanoparticle, further reducing the THz absorption. The average time for nanoparticle emptying thus appears as a separate time constant, τ_1 . This nanoparticle emptying time, Fig. 1(a) solid red circles, initially increases from 71 ps to 92 ps as pump fluence increases, and then becomes statistically invariant. The fraction of carriers leaving the nanoparticle, Fig. 1(b) solid red circles, decreases with increasing pump fluence, reaching 0 at $100 \mu\text{J}/\text{cm}^2$. Notably, the fraction of carriers leaving the nanoparticle decreases at a slower rate than carriers entering the nanoparticle. This suggests that the rate and number of carriers leaving the nanoparticles depend on the occupation of states in the surrounding matrix, and subsequently, that the recombination of electrons in the InGaAs conduction band and holes in the TbAs valence band is a significant emptying process. The fraction of carriers leaving the nanoparticle diminishes to zero for high pump fluences, suggesting saturation of the states around the nanoparticle that participate in the nanoparticle emptying process.

When the nanoparticles become saturated, carriers must find another relaxation mechanism. The solid blue triangles in Fig. 1(a) show that the relaxation time across the bulk band gap increases with pump fluence, ranging from 766 ps to 44.2 ns, approaching the bulk lifetime of InGaAs.¹⁷ This increased lifetime can be attributed to the saturation of both TbAs and other defects in the material. The solid blue triangles in Fig. 1(b) show that the fraction of carriers relaxing across the InGaAs band gap increases with pump fluence and is one at $100 \mu\text{J}/\text{cm}^2$. At high pump fluences the finite number of nanoparticle states and number of matrix to nanoparticle trap emptying states are saturated, and the excess carriers must relax across the bulk band gap.

There are many similarities in the carrier dynamics between the TbAs:InGaAs system and the previously measured TbAs:GaAs system.¹⁵ Both systems have similar relaxation times of carriers into the nanoparticle and emptying times of the nanoparticles. The emptying of the nanoparticles in both matrices depends on the occupation of carriers in the surrounding matrix. Finally, the percentage of carriers entering and leaving the nanoparticles decreases with increasing pump fluence, suggesting a band gap within the nanoparticle. The major difference in these two systems, however, is that the fraction of carriers entering and leaving the TbAs nanoparticles in the TbAs:InGaAs system reached zero during this measurement, indicating complete saturation of the nanoparticles, while the nanoparticles in the TbAs:GaAs system have not saturated. The saturation difference cannot be explained by only accounting for the difference in nanoparticle density. The TbAs:InGaAs system shows complete saturation at a pump fluence of $20 \mu\text{J}/\text{cm}^2$. If only the nanoparticle density determined the saturation rate, the TbAs:GaAs system should saturate at a pump fluence of $25 \mu\text{J}/\text{cm}^2$. Complete saturation of the τ_1 process in the TbAs:GaAs system is not seen for any pump fluence measured, suggesting that differences in the trapping dynamics,

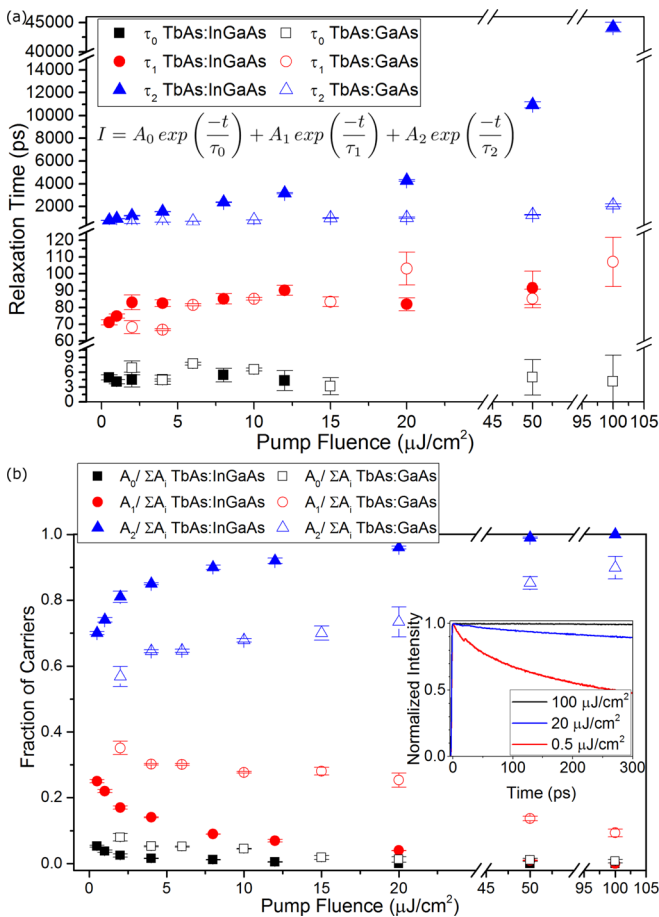


FIG. 1. (a) The relaxation time of each of the three processes (relaxation into the nanoparticles shown as black squares, emptying in the nanoparticles shown as red circles, and relaxation across the matrix's band gap shown as blue triangles) as a function of pump fluence is shown for the TbAs:InGaAs sample (solid symbols) and the TbAs:GaAs sample (hollow symbols). The inset shows the three exponential equations used to fit the decay in THz absorption. (b) The fraction of carriers participating in each relaxation process as a function of pump fluence is shown for both the TbAs:InGaAs sample and the TbAs:GaAs sample. The inset shows the exponential decay in THz absorption for the TbAs:InGaAs sample as a function of time, depicting the need for triple (red), double (blue), and single (black) exponential fits.

likely from differences in the band alignment, are causing the difference in saturation.

Given that TbAs nanoparticles have a band gap and the band alignment affects the trapping dynamics, the next step toward proposing a band alignment is obtaining the energy of transitions within the system. The absorption energies were obtained using spectrophotometry. Transmission and reflection spectra were collected with a Perkin Elmer Precisely Lambda 750 UV/Vis Spectrometer. Photoluminescence measurements,¹⁶ consistent with theoretical predictions, suggest that a TbAs band gap would be indirect. Thus, a Tauc plot for indirect band gap materials was used to determine absorption energies, Fig. 2.¹⁸ This absorption energy can be an interband transition within the nanoparticle or a transition from the nanoparticle to the matrix. The measured absorption energy is 0.61 ± 0.01 eV for the TbAs:GaAs system and 0.37 ± 0.03 eV for the TbAs:InGaAs system.

The Fermi level position is also needed for a band alignment diagram, and is estimated using temperature dependent Hall effect. These measurements were performed using a custom-built Hall effect system with indium contacts in the van der Pauw geometry. Data were collected from 45 K to 430 K, averaged at each temperature, and the resistivity, mobility, and carrier concentration were calculated. Figure 3 shows the free electron concentration for both films. The free electron concentration of the TbAs:GaAs film has a clear exponential temperature dependence above 315 K. Below 315 K the free electron concentration is level at approximately $2.5 \times 10^{12} \text{ cm}^{-3}$. This is attributed to the unintentional doping of the GaAs matrix. Fitting the temperature dependent free electron concentration to the relation $n = N_c \exp(E_a/kT)$ provides an activation energy, E_a , which corresponds to the chemical potential relative to the conduction band,¹⁹ and a reasonable estimate of the Fermi level.⁶ The resulting chemical potential is 0.66 eV below the conduction band edge. The TbAs:InGaAs film, however, is degenerate and shows a minimal temperature dependence that may be due to band bending at the matrix nanoparticle interface. Using a Fermi-Dirac fit, the Fermi level was calculated to be ~ 76 meV above the conduction band edge.

The combination of the measurements discussed above show that a type I (straddling) heterojunction in both systems

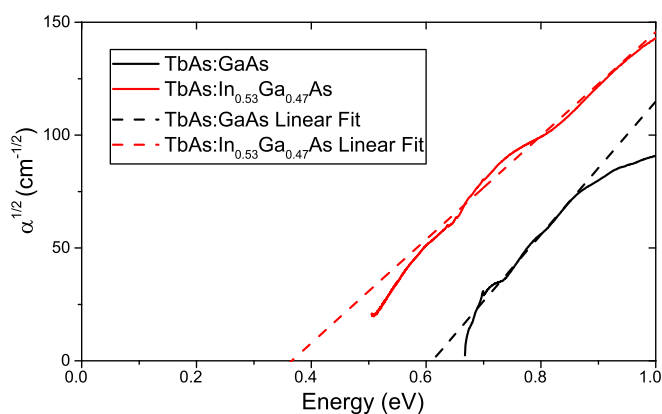


FIG. 2. A Tauc plot for an indirect absorption with the linear fits (dashed lines) was used to calculate an absorption energy of 0.61 ± 0.01 eV for the TbAs:GaAs system (black) and 0.37 ± 0.03 eV for the TbAs:InGaAs (red) system. Note that the detector cuts out for energies below 0.5 eV.

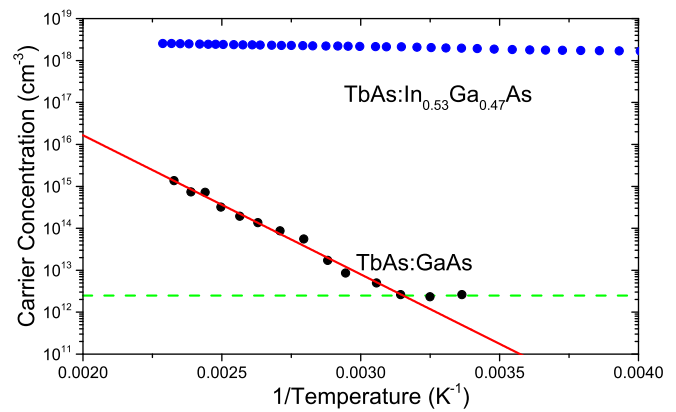


FIG. 3. Free electron concentration of the TbAs:GaAs (black dots) strongly depends on temperature, until unintentional doping (green dashed line) dominates, allowing an exponential fit (red line) to estimate a Fermi level. The degenerate TbAs:InGaAs (blue dots) has little temperature dependence.

is unphysical. If both systems had a type I alignment, the large blue shift in absorption (0.25 eV) that occurs when changing the matrix would require a change of ground state energy with confinement which is not consistent with any reasonable combination of TbAs band gap and effective mass. Instead, we propose that TbAs nanoparticles make a type I heterojunction with GaAs and a type II (staggered) heterojunction with InGaAs. A schematic of this band alignment is shown in Fig. 4.

The proposed band alignment is supported by the various data. Optical-pump THz-probe measurements show that the TbAs nanoparticles have a band gap, which is seen in the band alignment diagram, and that the two systems have different trapping dynamics. The type II heterojunction in the InGaAs system causes the TbAs nanoparticle to only trap holes. This change in trap behaviour would explain the saturation of the InGaAs sample at a lower fluence when compared to the GaAs sample.¹⁵ Spectrophotometry measurements provide two different absorption energies, 0.61 eV in the TbAs:GaAs system and 0.37 eV in the TbAs:InGaAs system. The type I band alignment in the TbAs:GaAs systems shows that the absorption feature is within the TbAs nanoparticle, indicating that the TbAs nanoparticle has a band gap somewhat smaller than 0.61 eV. The type II band alignment in the TbAs:InGaAs means the absorption transition is due to the excitation of electrons from the TbAs valence band to the Fermi level in the InGaAs matrix. Excitation of carriers must be above the Fermi level rather than the conduction band because the system is degenerate, as shown by the Hall effect data. The type II heterojunction would allow for band bending at the nanoparticle-matrix interface, creating a small two-dimensional electron gas in the InGaAs and a small barrier for electrons entering the matrix from the TbAs conduction band. Band bending explains the small temperature dependence of the free electron concentration shown with the Hall effect measurement.

In summary, we have proposed a band alignment for TbAs nanoparticles embedded within GaAs and InGaAs that is consistent with all available optical and electronic measurements. Optical-pump THz-probe measurements provide the carrier relaxation dynamics, which depend on band alignment, and show that the TbAs nanoparticles are saturable

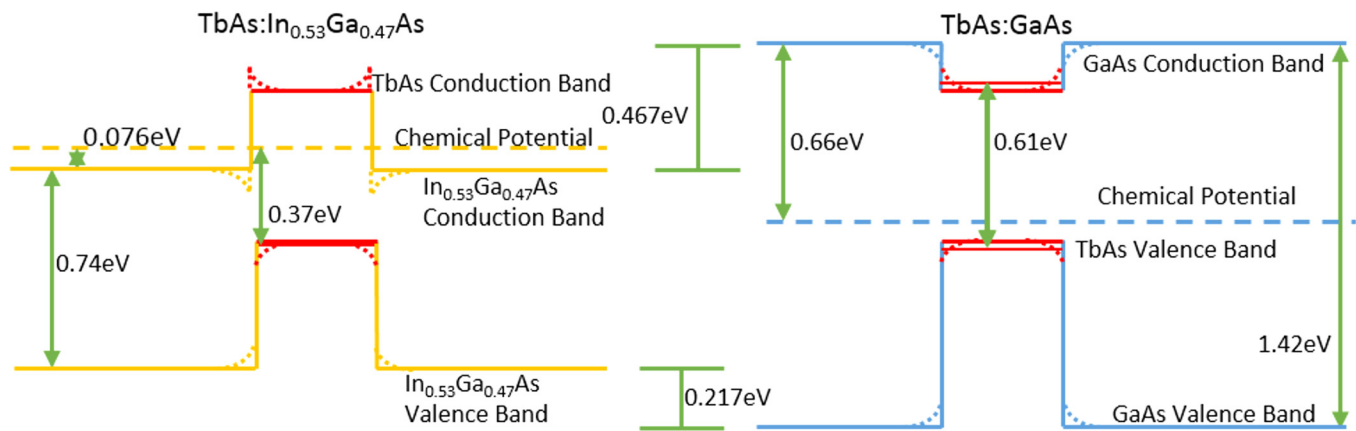


FIG. 4. Schematic showing the proposed band alignments of TbAs nanoparticles (red) in InGaAs (yellow) and GaAs (blue). Energy offsets are shown with green arrows, dashed lines represent the nanocomposite's estimated Fermi level, thin lines represent the first energy level within the nanoparticle, thick lines represent band edges, and dotted lines represent exaggerated band bending at the nanoparticle matrix interface. Note that all energies involving the TbAs nanoparticle are relative to the first energy level; the conduction and valence band edges of TbAs are only included as an estimate.

and likely have a band gap. Using spectrophotometry, we find that the minimum energy required to generate an electron hole pair is 0.61 eV for the TbAs:GaAs system and 0.37 eV for the TbAs:InGaAs system. Finally, Hall effect measurements estimate the Fermi level to be pinned 0.61 eV below the conduction band edge in the TbAs:GaAs system and 76 meV above the conduction band edge of the TbAs:InGaAs system. Combining all of these measurements, we propose that the TbAs nanoparticles form a type I heterojunction with GaAs and a type II heterojunction with InGaAs.

The authors wish to acknowledge the support from the National Science Foundation (DMR-1105137). Additionally, usage of facilities at Los Alamos National Laboratory (LANL) was made possible by the Center for Integrated Nanotechnology (CINT), a Department of Energy Basic Energy Science user facility. The authors also acknowledge the partial support from LANL-LDRD program.

¹W. Kim, J. M. O. Zide, A. Gossard, D. Klenov, S. Stemmer, A. Shakouri, and A. Majumdar, *Phys. Rev. Lett.* **96**, 045901 (2006).

²L. E. Clinger, G. Pernot, T. E. Buehl, P. G. Burke, A. C. Gossard, C. J. Palmström, A. Shakouri, and J. M. O. Zide, *J. Appl. Phys.* **111**, 094312 (2012).

³J. M. O. Zide, A. Kleiman-Shwarscstein, N. C. Strandwitz, J. D. Zimmerman, T. Steenblock-Smith, A. C. Gossard, A. Forman, A. Ivanovskaya, and G. D. Stucky, *Appl. Phys. Lett.* **88**, 162103 (2006).

⁴H. P. Nair, A. M. Crook, and S. R. Bank, *Appl. Phys. Lett.* **96**, 222104 (2010).

⁵J. F. O'Hara, J. M. O. Zide, A. C. Gossard, A. J. Taylor, and R. D. Averitt, *Appl. Phys. Lett.* **88**, 251119 (2006).

⁶R. Salas, S. Guchhait, S. D. Sifferman, K. M. McNicholas, V. D. Dasika, E. M. Krivoy, D. Jung, M. L. Lee, and S. R. Bank, *Appl. Phys. Lett.* **106**, 081103 (2015).

⁷P. B. Dongmo, M. Hartshorne, T. R. Cristiani, M. L. Jablonski, C. C. Bomberger, D. Isheim, D. N. Seidman, M. L. Taheri, and J. M. O. Zide, *Small* **10**, 4920 (2014).

⁸D. C. Driscoll, M. Hanson, C. Kadow, and A. C. Gossard, *Appl. Phys. Lett.* **78**, 1703 (2001).

⁹K. T. Delaney, N. A. Spaldin, and C. G. Van de Walle, *Phys. Rev. B* **81**, 165312 (2010).

¹⁰J. M. O. Zide, J. H. Bahk, R. Singh, M. Zebarjadi, G. Zeng, H. Lu, J. P. Feser, D. Xu, S. L. Singer, Z. X. Bian, A. Majumdar, J. E. Bowers, A. Shakouri, and A. C. Gossard, *J. Appl. Phys.* **108**, 123702 (2010).

¹¹J. M. O. Zide, D. O. Klenov, S. Stemmer, A. C. Gossard, G. Zeng, J. E. Bowers, D. Vashaee, and A. Shakouri, *Appl. Phys. Lett.* **87**, 112102 (2005).

¹²J. K. Kawasaki, R. Timm, K. T. Delaney, E. Lundgren, A. Mikkelsen, and C. J. Palmström, *Phys. Rev. Lett.* **107**, 036806 (2011).

¹³M. A. Scarpulla, J. M. O. Zide, J. M. LeBeau, C. G. Van De Walle, A. C. Gossard, and K. T. Delaney, *Appl. Phys. Lett.* **92**, 173116 (2008).

¹⁴M. Said, C. Bertoni, A. Fasolino, and S. Ossicini, *Solid State Commun.* **100**, 477 (1996).

¹⁵L. R. Vanderhoef, A. K. Azad, C. C. Bomberger, D. R. Chowdhury, D. B. Chase, A. J. Taylor, J. M. O. Zide, and M. F. Doty, *Phys. Rev. B* **89**, 045418 (2014).

¹⁶L. E. Cassels, T. E. Buehl, P. G. Burke, C. J. Palmström, A. C. Gossard, G. Pernot, A. Shakouri, C. R. Haughn, M. F. Doty, and J. M. O. Zide, *J. Vac. Sci. Technol.*, **B 29**, 03C114 (2011).

¹⁷R. K. Ahrenkiel, R. Ellingson, S. Johnston, and M. Wanlass, *Appl. Phys. Lett.* **72**, 3470 (1998).

¹⁸J. I. Pankove, *Optical Processes in Semiconductors*, edited by N. Holonyak, Jr. (Prentice-Hall, INC., Englewood Cliffs, NJ, 1971), pp. 37–42.

¹⁹N. W. Ashcroft and N. D. Mermin, *Solid State Physics* (Holt, Rinehart and Winston, New York, 1976), pp. 572–574.